ROYAL SOCIETY
OF CHEMISTRY

EDGE ARTICLE

Check for updates

Neutral anion-detecting organic cages based on anion–π interactions

Yuyang Lu,†[a] Ping Zhou,†[ab] Hua Tang,†[a] Yating Wu,[a] Yueyan Kuang,[a] Ze Cao,[a] Jiyong Liu,[d] Guangcheng Wu,*[e] Hongliang Chen [iD] *[abc] and Hao Li [iD] *[ab]

A series of neutral tetrahedral molecular cages were self-assembled in relatively high yields by condensing a triamino linker with triangular tris-aldehyde precursors. Each tris-aldehyde features a central triazine core, which imparts an electron-deficient cavity that facilitates anion encapsulation through fourfold anion–π interactions. The anion binding affinity is significantly influenced by substituents on the tris-aldehyde precursors: electron-donating groups (*e.g.*, Ph) diminish binding by compromising the electron-deficient nature of the cage, whereas more electron-withdrawing substituents (*e.g.*, Cl, Br, and CF₃-Ph) enhance it. Interestingly, the strongly electron-withdrawing fluorine (F) substituents, in close proximity to the binding pocket, unexpectedly diminish binding affinity due to a repulsive field effect. Within each corner of the tetrahedral framework, intramolecular CH–π interactions occur between a phenyl proton *ortho* to the imine bond and an adjacent phenyl plane. The encapsulation of anionic guests within the cavity perturbed or reinforced these CH–π interactions to varying degrees, producing distinct NMR responses that serve as signatures for different anions.

Introduction

The recognition and detection of anions represent a major focus in supramolecular chemistry due to their critical roles in nature, such as metabolic regulation,[1,2] aquatic eutrophication,[3,4] and the maintenance of physiological homeostasis.[5,6] A common approach of anion detection involves designing artificial anion acceptors that can bind with anionic targets by leveraging hydrogen bonding,[7–16] halogen bonding,[17–26] electrostatic forces,[27] hydrophobic effects,[28–32] and coordination to metal ions[33–36] or boron atoms[37] developed more recently. However, another type of weak supramolecular force—anion–π interaction[38–41]—was long overlooked in host–guest chemistry. This changed a few decades ago when some theoretical chemists proposed[42–44] the feasibility of using electron-deficient π systems to bind negatively charged species (Fig. 1A). Typically, the so-called anion–π interactions are weaker in strength than commonly employed interactions including hydrogen

bonds.[45,46] As a consequence, anion–π interactions can hardly be used as the primary binding forces that solely drive guest recognition in the absence of other noncovalent forces. For example, many groups obtained[47–50] various coordination cages bearing triazine walls, whose cavities can encapsulate anions. Here, electrostatic forces resulting from metal cations and anion–π interactions act as the primary and secondary driving forces, respectively, as inferred from the results that anion recognition can still occur even after the triazine units were replaced with electron rich phenyls.[51,52] Developing neutral anion-detecting probes, in which anion–π interactions play the predominant roles, still needs to be exploited. Additionally, unlike hydrogen bonds, which exhibit partial covalent character and induce noticeable shifts in proton NMR spectra, anion–π interactions arise from electrostatic forces and usually result in minimal or no shifts[53] in the corresponding ¹H NMR spectra, unless hydrogen bonding is also involved.[54] Other techniques for probing anion–π interactions also face limitations, including (i) crystallography,[55] which only confirms binding in the solid state; (ii) mass spectrometry,[56] which provides limited quantitative information; and (iii) UV-Vis absorption and fluorescence[57] spectroscopies, which require dramatically different spectra for hosts and the corresponding host–anion complexes, a condition not always met. Therefore, it remains a key challenge to develop artificial hosts with high synthetic efficiency and the ability to produce distinct NMR responses for different anions as their signatures.

In our group, a variety of complex molecules[58] were synthesized through reversible organic reactions, including imine

[a]*Stoddart Institute of Molecular, Science Department of Chemistry, Zhejiang University, Hangzhou 310058, China. E-mail: lihao2015@zju.edu.cn; hongliang.chen@zju.edu.cn*

[b]*Zhejiang-Israel Joint Laboratory of Self-Assembling Functional Materials, ZJU-Hangzhou Global Scientific and Technological Innovation Center, Zhejiang University, Hangzhou 311215, China*

[c]*Beijing National Laboratory for Molecular Sciences, Beijing 100871, China*

[d]*Department of Chemistry, Zhejiang University, Hangzhou 310058, China*

[e]*Department of Chemistry, The University of Hong Kong, Hong Kong SAR, 999077, China. E-mail: gcwu2023@hku.hk*

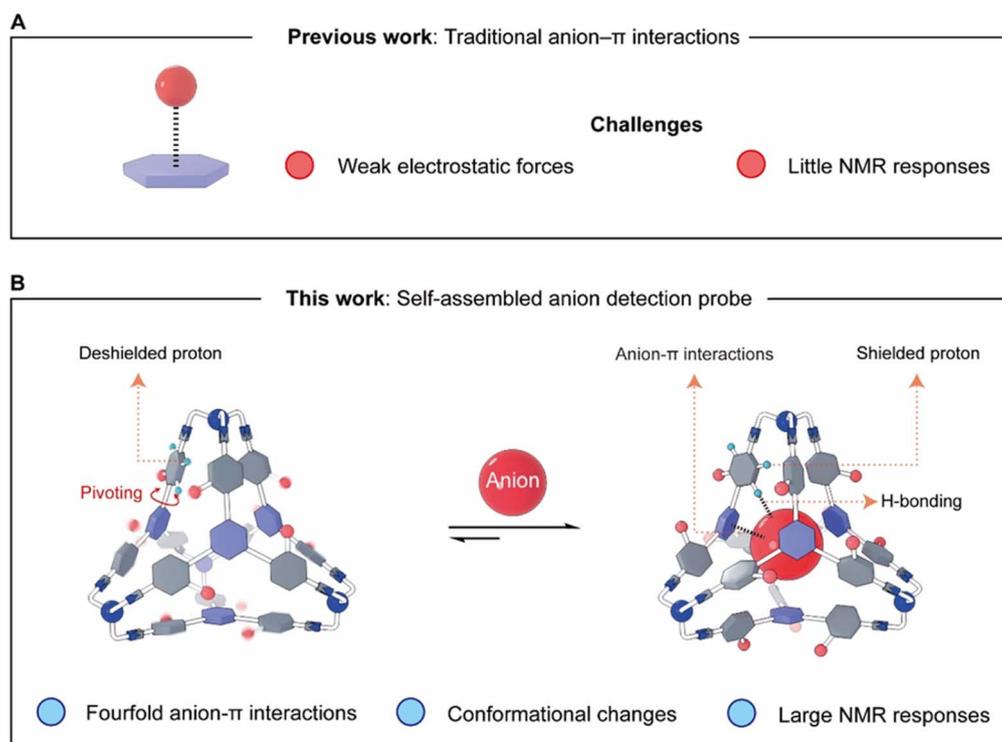† Y. L., P. Z., and H. T. contributed equally to this work.

Fig. 1 Graphical representations of (A) a traditional electron-deficient π system engaging in an anion−π interaction, and (B) a self-assembled cage encapsulating an anion *via* fourfold anion−π interactions in CDCl$_3$. The preorganized cage architecture in (B) enhances binding affinity relative to the open system in (A), *via* a combination of many supramolecular forces including anion−π interactions and hydrogen bonds. Anion encapsulation induces conformational changes in the cage, resulting in significant NMR chemical shift changes for protons that experience altered chemical environments.

bond formation, which allows for error correction. For example, a series of tetrahedral molecules[59–63] were self-assembled by condensing four equivalents of the trisamino linker tris(2-aminoethyl)amine (TREN) as the vertices with four equivalents of various trisformyl precursors as the faces. In some cases, the yields of these tetrahedral cages are nearly quantitative, partially due to the stabilizing intramolecular CH−π interactions at each tetrahedral corner between an *ortho*-phenyl proton (relative to an imine bond) and the adjacent phenyl moiety. The critical role that CH−π interactions play in driving the formation of tetrahedra was confirmed by a control experiment in which, when one of the *ortho*-phenyl protons was replaced by other nonacidic unit, including F, the tetrahedral cages cannot form.[61] None of these tetrahedral cages exhibit the ability to accommodate anions, due to the electron rich nature of the phenyl building blocks. We propose that replacing the phenyl units on the faces with electron-deficient triazine moieties could generate a tetrahedron whose cavity is capable of anion recognition *via* fourfold anion−π interactions (Fig. 1B) in the absence of electrostatic attraction.

Results and discussion

A series of trisformyl precursors each with a central triazine core **1a**–**1f** (Fig. 2) were obtained either through commercial purchase or synthesis. The commercially available **1a** was first combined with TREN in CDCl$_3$ in a 1 : 1 ratio. The solution was heated at 55 °C for 12 h to allow imine formation to reach equilibrium. However, the ^{1}H NMR spectrum indicated that the expected tetrahedron **2a** was not produced. Instead, a triangular prism-shaped molecule (**3a**) was self-assembled within a library of mixture, consistent with our previously reported results.[64] The failure of tetrahedron formation stems from the fact that the tetrahedron formation requires the occurrence of CH−π interactions as the driving force, which necessitates that each benzaldehyde unit adopts an edge-in conformation. Given that the central triazine core orientates in a face-in manner within the tetrahedron framework, this in turn forces each benzaldehyde unit to twist into a specific dihedral angle relative to the central triazine unit. Unfortunately, **1a** has a planar conformation, stabilized by intramolecular CH−N hydrogen bonds and phenyl-triazine conjugation. This conformational difference between the precursor **1a** and the putative product **2a** implies an energetic penalty that disfavors tetrahedron formation.

1b–**1f** are derivatives of **1a**, each bearing a functional group at the *meta*-position relative to the formyl unit of the benzaldehyde function, including F (**1b**), Cl (**1c**), Br (**1d**), Ph (**1e**), and 4-CF$_3$Ph (**1f**). These substituents introduce either steric hindrance or coulombic repulsion, thereby forcing each benzaldehyde unit to adopt a twisted dihedral angle relative to the triazine core. We thus proposed that the more twisted conformations of the
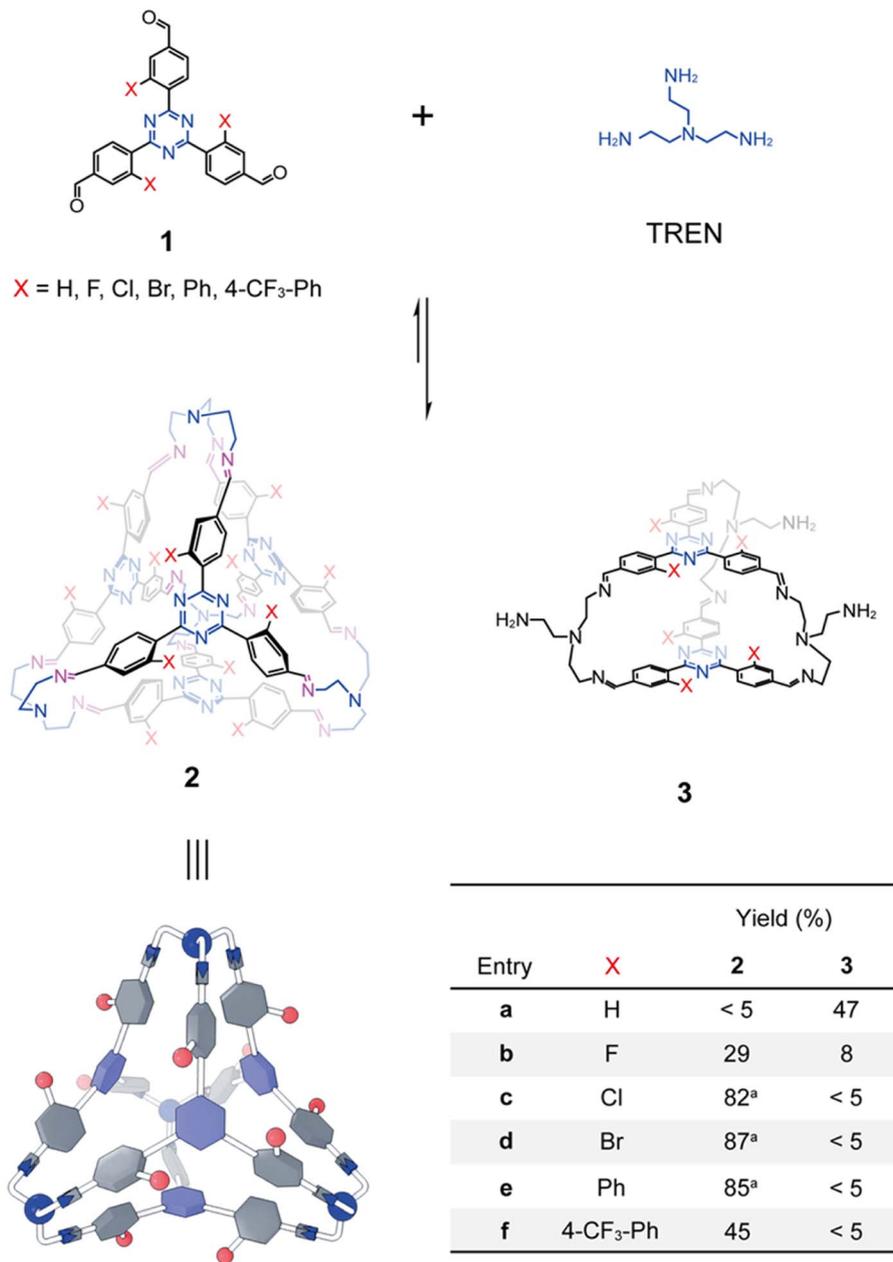
X = H, F, Cl, Br, Ph, 4-CF₃-Ph

Fig. 2 Structural formulae of tetrahedral cages (**2a–2f**) and prisms (**3a–3f**) obtained from the condensation of triformyl precursors (**1a–1f**) with the triamino linker, TREN. Yields are provided in the table at the bottom right. [a]Yields for **2c**, **2d**, and **2e** are isolated; all others were determined by integration of product resonances in their *in situ* ^{1}H NMR spectra relative to an internal standard. A yield of <5% indicates the product was not observed in the corresponding ^{1}H NMR spectrum.

Entry	X	Yield (%)	
		2	**3**
a	H	< 5	47
b	F	29	8
c	Cl	82[a]	< 5
d	Br	87[a]	< 5
e	Ph	85[a]	< 5
f	4-CF₃-Ph	45	< 5

trisformyl precursors **1b–1f** relative to **1a** might favor the formation of the corresponding tetrahedral products. The F-substituents in **1b**, being the smallest non-hydrogen atom, endow this precursor with the smallest twisting dihedral angle. It is thus predictable that the formation of the tetrahedron **2b** would be favored to the least extent. This hypothesis was confirmed, as a 1 : 1 mixture of **1b** and TREN produced both tetrahedron **2b** and prism **3b** in a 2 : 1 manner, which was indicated by the ^{1}H NMR spectrum (see Fig. S32 in the SI). By comparing the integrations of the corresponding resonances of

the products and the formyl precursor relative to an internal standard, the cyclization yields of **2b** and **3b** were calculated to be around 29% and 8%, respectively.

As a comparison, combination of each of **1c–1f** with TREN in CDCl₃ produced only the corresponding tetrahedra **2c–2f** as the sole observable products in their ^{1}H NMR spectra (see the SI), further confirming that their preorganized twisted conformations are of importance in self-assembly, by favoring the occurrence of the CH–π interactions. **2c**, **2d** and **2e** were isolated as solid-state compounds *via* precipitation by adding

petroleum ether into the corresponding self-assembly solutions (see the detailed procedures in the SI). The isolated yields of **2c**, **2d** and **2e** were determined to be 82%, 87% and 85%, respectively. These cages were re-dissolved in CDCl$_3$ and their ^{1}H NMR spectra were recorded, confirming their purity and indicating that **2c**, **2d** and **2e** are rather stable or kinetically inert during precipitation, despite the dynamic nature of imine formation. Attempts to isolate **2f** using the same procedure were unsuccessful. The ^{1}H NMR spectrum recorded after precipitation showed a few resonances corresponding to impurities that were not detected in the *in situ* self-assembly solution, suggesting

partial degradation of **2f** during precipitation. Therefore, the *in situ* self-assembly solution of **2f** was used for the following host–guest binding investigations. The cyclization yield of **2f** was determined to be 45% by using an internal standard. The relatively low yield of **2f** compared with other cage products was due to the production of some insoluble byproducts, which might be oligomers or polymers. Luckily, **2f** is the only observable product in the ^{1}H NMR spectrum, which can be used for host–guest recognition without further purification.

In the ^{1}H NMR spectrum of **2c** (Fig. 3B), the resonances corresponding to the protons a and c in the *ortho* positions
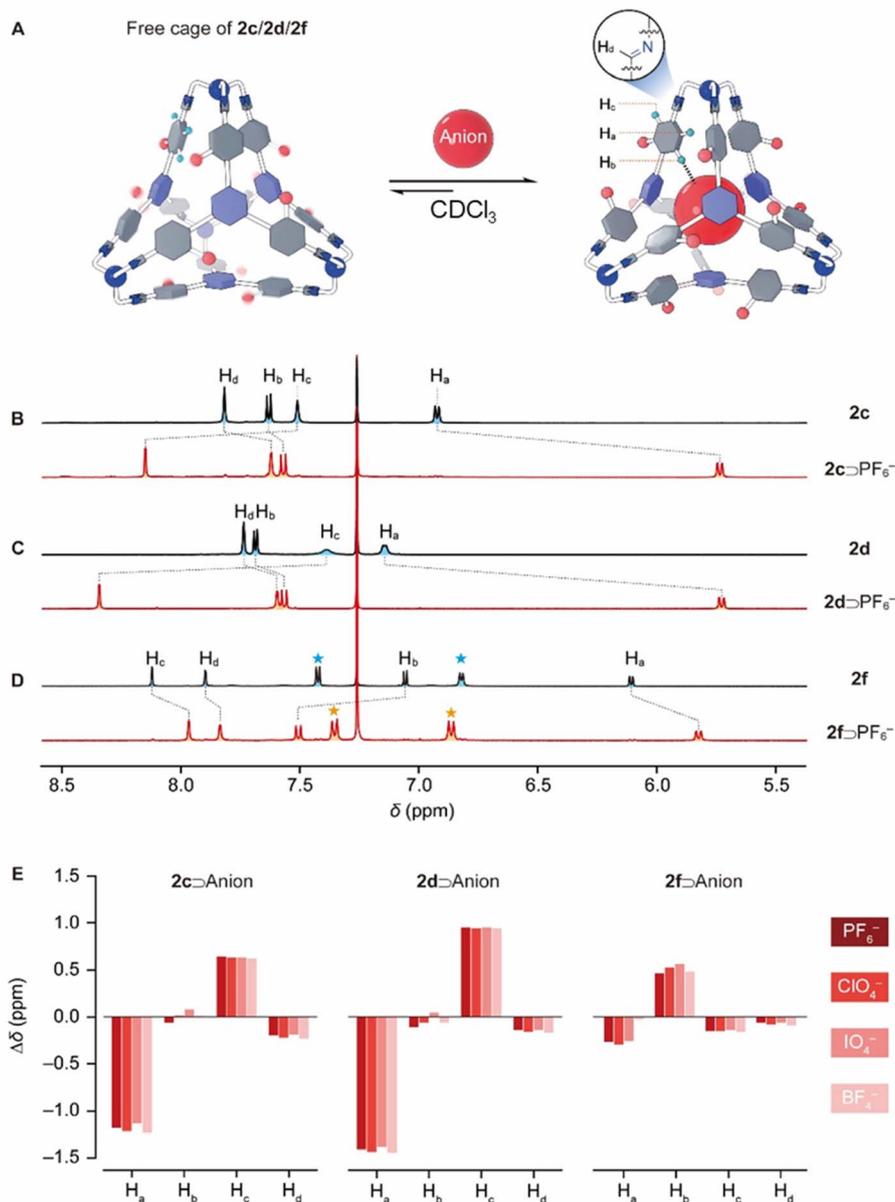

Fig. 3 (A) Graphical representation of cages **2c**, **2d**, and **2f** encapsulating an anionic guest. Partial ^{1}H NMR spectra (400 MHz, CDCl$_3$, 298 K) of (B) **2c**, (C) **2d**, and (D) **2f** before (top, black trace) and after (bottom, red trace) encapsulation of a PF$_6^-$ guest. In (D), resonances marked with blue and orange asterisks correspond to protons on the 4-CF$_3$Ph substituents of **2f**. (E) Chemical shift changes (Δδ, ppm) for protons H$_a$–H$_d$ in the host–guest complexes of anion⊂**2c** (left), anion⊂**2d** (middle), and anion⊂**2f** (right) relative to the corresponding "free" cages namely **2c**, **2d** and **2f**, respectively. Proton assignments are provided in (A).

relative to the imine bond were observed at around 6.93 and 7.82 ppm, which shifted upfield by 1.04 and 0.59 ppm, respectively, compared to the precursor **1c**. These substantial upfield shifts for both protons confirm that each experiences a shielded magnetic environment due to intramolecular CH–π interactions with an adjacent phenyl moiety within the cage framework. The ^{1}H NMR spectra of **2b** and **2d** exhibited similar patterns, except that in **2d**, the resonances corresponding to protons a and c became relatively broad (Fig. 3C), indicating that rotation within **2d** occurs at a slower rate compared to **2c**. This is attributed to the bulkier Br atom in **2d**, which introduces a higher energy barrier for rotation. In contrast, no rotation was observed in the framework of either **2e** or **2f**. In the ^{1}H NMR spectrum of **2e** (Fig. S47), the resonances corresponding to a and c appeared at 6.10 and 8.10 ppm, respectively, which are located in significantly upfield and downfield positions compared with their counterparts in **2c** or **2d**. This observation indicated that in **2e**, proton a is oriented inward toward the cage cavity while proton c is oriented outward, away from the cavity at all times – a conformation driven by the large phenyl substituent, which cannot fit within the cage cavity. The ^{1}H NMR spectrum of **2f** (Fig. 3D) is similar to that of **2e**, which is predictable given that its 4-CF$_3$Ph substituent is even bulkier.

Given that each tetrahedral cage contains four triazine units, we hypothesized that they are capable of recognizing anionic guests *via* fourfold anion–π interactions. Various commercially available anions, all introduced as tetrabutylammonium (TBA$^+$) salts, were added to CDCl$_3$ solutions of **2b**. Little or no changes were observed in the ^{1}H NMR spectra (Fig. S69), indicating that **2b** is incapable of recognizing any of these anions. In the case of **2c** and **2d**, addition of F$^-$, Cl$^-$, Br$^-$, I$^-$, H$_2$PO$_4$$^-$, NO$_3$$^-$, AcO$^-$ and SiF$_6$$^{2-}$, led to little or no changes in the corresponding ^{1}H NMR spectra (Fig. S57 and S62) either. These observations indicated that the cage either **2c** or **2d** has little or no binding towards these anions, probably because of these less complementary sizes or weaker anion–π interactions. Addition of HSO$_4$$^-$ led to degradation of **2c**. To our delight, addition of PF$_6$$^-$ to **2d** led to a concomitant attenuation of the resonances corresponding to the "free" cage and an increase of a new set of resonances corresponding to the complex PF$_6$$^-$⊂**2d**. After approximately six hours, no further change in the composition of the reaction mixture was observed, indicating that complexation of PF$_6$$^-$⊂**2d** had reached equilibrium. In the case of the complex PF$_6$$^-$⊂**2d**, the resonances corresponding to protons a and c were observed at 5.74 and 8.34 ppm, which shifted upfield and downfield by 1.41 and 0.95 ppm compared with those of the "free" cage **2d**, respectively (Fig. 3C, red trace). Apparently, these

pronounced resonance shifts resulted from the conformational rearrangements upon guest encapsulation: the anionic guest forced the Br atoms and proton c to orient outward, while forcing proton a to reside inward at all times. The binding constant (K_a) for PF$_6$$^-$⊂**2d** was evaluated to be $(5.6 \pm 0.5) \times 10^3$ M^{-1} (Table 1) by integrating the resonances corresponding to the "free" cage and the complex in the ^{1}H NMR spectrum of a mixture of PF$_6$$^-$ and **2d**. By performing similar experiments, a series of anionic complexes including ClO$_4$$^-$⊂**2d**, IO$_4$$^-$⊂**2d** and BF$_4$$^-$⊂**2d** were obtained. In their corresponding ^{1}H NMR spectra (Fig. S63–S66), the resonances corresponding to the proton a were observed to undergo upfield shifts by 1.44, 1.38 and 1.45 ppm, respectively (Fig. 3E, middle). The binding constants of ClO$_4$$^-$⊂**2d**, IO$_4$$^-$⊂**2d** and BF$_4$$^-$⊂**2d** were determined to be $(1.0 \pm 0.1) \times 10^3$, $(2.5 \pm 0.1) \times 10^2$ and $(1.6 \pm 0.1) \times 10^2$ M^{-1}, respectively (Table 1). All the above anionic guests were considered having little or no association with their counterion TBA$^+$ in chlorinated solvents due to their lower basicity.[65–67]

To investigate the influence of the solvophobic effect on binding constants, we also performed binding experiments in more polar solvents, namely CDCl$_3$/CD$_3$SOCD$_3$ (5 : 1, v/v). The NMR titration results (Fig. S64) revealed that the binding constant of PF$_6$$^-$⊂**2d** was significantly reduced from 5.6 ($\pm$0.5) $\times 10^3$ M^{-1} in pure CDCl$_3$ to 1.5×10^2 M^{-1} in CDCl$_3$/CD$_3$SOCD$_3$ (5 : 1, v/v). This experiment indicated that more polar solvent disfavored host–guest binding by shielding its charge and thus suppressing anion–π interactions. We thus reasonably hypothesize that the solvophobic effect might play a less dominant role compared with anion–π interactions in anion recognition. The cage **2c** bearing Cl atoms exhibited similar binding behaviors. In the ^{1}H NMR spectra of the complexes PF$_6$$^-$⊂**2c**, ClO$_4$$^-$⊂**2c**, IO$_4$$^-$⊂**2c** and BF$_4$$^-$⊂**2c** (Fig. S58–S61), the resonances corresponding to proton a underwent upfield shifts by 1.18, 1.22, 1.14 and 1.23 ppm, respectively (Fig. 3E, left), relative to the "free" **2c**. The corresponding binding constants for these complexes were determined to be $(8.2 \pm 0.3) \times 10^2$, $(2.2 \pm 0.1) \times 10^2$, $(7.0 \pm 0.7) \times 10^1$ and $(3.0 \pm 0.4) \times 10^1$ M^{-1}, respectively (Table 1).

The addition of these anions with TBA$^+$ counterions to the CDCl$_3$ solutions of **2e** led to little or no shifts (Fig. S70). This outcome is somewhat surprising considering that the framework of **2e** is identical to that of either **2c** or **2d**, aside from the different substituents. One possible explanation is that the phenyl substituents in the framework of **2e** introduced steric hindrance to the anionic guests, increasing the energy barriers for host–guest association. This possibility was ruled out by the

Table 1 Association constants K_a for each of the hosts **2b**–**2f** to recognize the anions. N. D. = not determined *via* ^{1}H NMR spectroscopy, because the corresponding K_a values are too small to be measured

K_a (M^{-1})	2b	2c	2d	2e	2f
PF$_6$$^-$	N. D.	8.2 ($\pm$0.3) × 10^2	5.6 ($\pm$0.5) × 10^3	N. D.	5.7 ($\pm$0.4) × 10^3
ClO$_4$$^-$	N. D.	2.2 ($\pm$0.1) × 10^2	1.0 ($\pm$0.1) × 10^3	N. D.	1.1 ($\pm$0.3) × 10^3
IO$_4$$^-$	N. D.	7.0 ($\pm$0.7) × 10^1	2.5 ($\pm$0.1) × 10^2	N. D.	1.2 ($\pm$0.2) × 10^3
BF$_4$$^-$	N. D.	3.0 ($\pm$0.4) × 10^1	1.6 ($\pm$0.1) × 10^2	N. D.	9.0 ($\pm$0.7) × 10^1

experiments that the combination of **1e** and TREN in the presence of the putative anionic guests produced the "free" cage **2e** exclusively (Fig. S71). Another explanation is that the phenyl substituents in **2e** are relatively electron-rich, which jeopardized the electron deficient nature of the cage **2e**. We thus synthesized **2f**, an analogue of **2e** with more electron-withdrawing 4-CF$_3$Ph units, and tested its anion recognition ability. After adding these anions to the solution of **2f**, we observed the formation of host–guest complexes, as evidenced by shifts in the ^{1}H NMR spectra, although the complexation did not reach equilibrium until a few days. Therefore, the complexes PF$_6^-$⊂**2f**, ClO$_4^-$⊂**2f**, IO$_4^-$⊂**2f** and BF$_4^-$⊂**2f** were successfully obtained by self-assembling the cage **2f** in the presence of these anionic guests as templates. In the ^{1}H NMR spectra (Fig. 3D and S71–S74) of these complexes, the resonances corresponding to proton a underwent upfield shifts by 0.27, 0.29, 0.26 and 0.30 ppm (Fig. 3E, right), respectively, relative to the "free" **2f**. These upfield shifts imply an enhanced shielded magnetic effect occurred to the protons a in the complexes compared with the "free" cage **2f**. One possible explanation is that the accommodation of anionic guests leads to the expulsion of a solvent molecule (CDCl$_3$) from the cage cavity, causing the cage

framework to shrink slightly and enhanced CH–π interactions. It is noteworthy that the upfield shifts in **2f** were less pronounced than those observed in **2c** and **2d**. This can be attributed to the fact that **2f** undergoes fewer conformational changes during anion accommodation, *i.e.*, the protons a are forced to reside inside the cage cavity by the 4-CF$_3$Ph substituents regardless of whether anions are present. K_a values of PF$_6^-$⊂**2f**, ClO$_4^-$⊂**2f**, IO$_4^-$⊂**2f** and BF$_4^-$⊂**2f** were determined to be $(5.7 \pm 0.4) \times 10^3$, $(1.1 \pm 0.3) \times 10^3$, $(1.2 \pm 0.2) \times 10^3$ and $(9.0 \pm 0.7) \times 10^1$ M^{-1}, respectively (Table 1), by integrating the corresponding resonances for both the complexes and the "free" cage.

The ability of cages **2c**, **2d**, and **2f** to produce distinct NMR responses for different anions encouraged us to test their utility as probes to detect multiple anions simultaneously when they are present as a mixture (Fig. 4A). A mixture of TBA$^+$ salts of PF$_6^-$, BF$_4^-$, ClO$_4^-$, and IO$_4^-$ (each at 3 mM) was added to a CDCl$_3$ solution of **2d** (0.5 mM). After the host–guest complexes reached equilibrium, the ^{1}H NMR spectrum was recorded. The resonances corresponding to all four complexes namely PF$_6^-$⊂**2d**, ClO$_4^-$⊂**2d**, IO$_4^-$⊂**2d** and BF$_4^-$⊂**2d** were clearly observed (Fig. 4B). However, for some unknown reasons, the
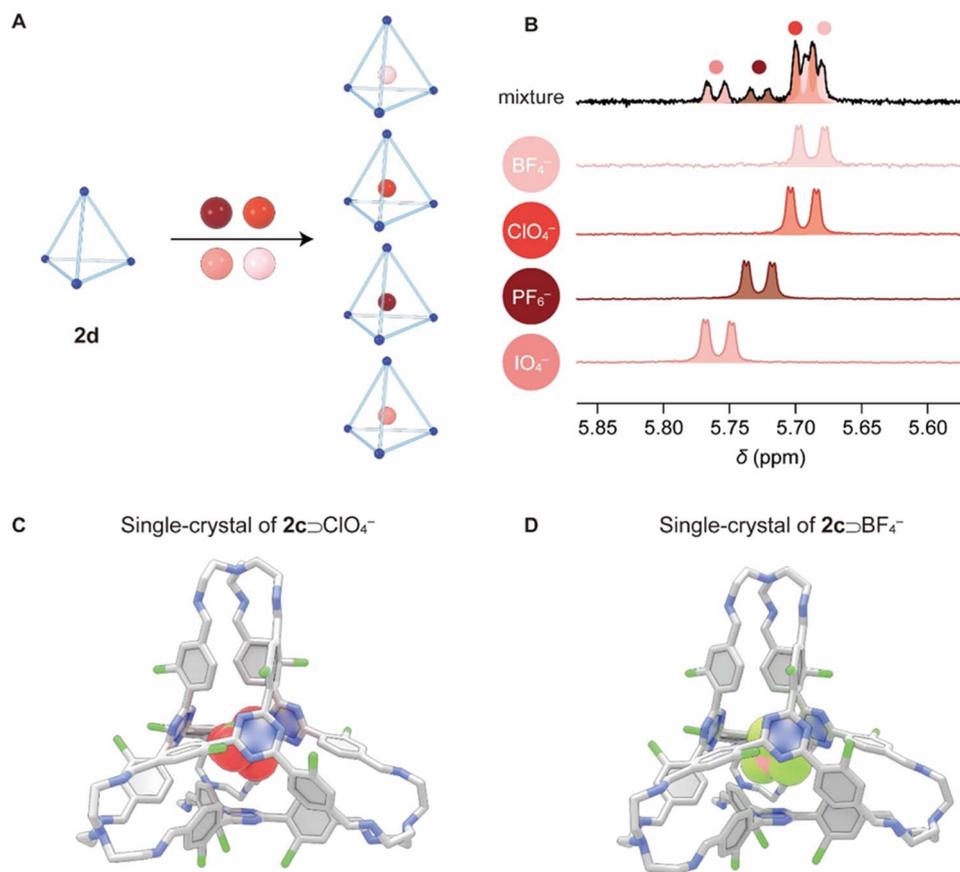

Fig. 4 (A) Graphical representation of cage **2d** encapsulating four different anions. (B) Partial ^{1}H NMR spectra (400 MHz, CDCl$_3$, 298 K) of **2d** (0.5 mM) after the addition of a mixture of PF$_6^-$, ClO$_4^-$, IO$_4^-$ and BF$_4^-$ (top), each at a concentration of 3 mM, and after the addition of each individual anion (below). The full spectra are shown in the SI. All anions were added as their TBA$^+$ salts. Side views of the core structures from single-crystal X-ray diffraction analysis for (C) ClO$_4^-$⊂**2c** and (D) BF$_4^-$⊂**2c**. Color code: carbon, gray; nitrogen, blue; chlorine, green; oxygen, red; boron, orange; fluorine, light green. TBA$^+$ counterions, hydrogen atoms, and solvent molecules are omitted for clarity.

NMR integral ratios corresponding to different complexes do not match the binding constants. The probing ability is a key advantage resulting from the confined cavity of **2d**, which led to slow exchange between the "free" cage and each of the different complexes on the timescale of ^1H NMR spectroscopy. Such discrimination is typically unattainable in traditional systems with "open" structures, such as those reported by Wang,[68,69] where complexes undergo fast association/dissociation exchange on the NMR timescale, leading to averaged signals for mixtures. The ability of our cage systems to detect multiple anions within a library of mixture simultaneously is reminiscent of the bambusuril rings reported by Sindelar et al.[70]

To gain a more quantitative understanding of the kinetic parameters controlling the formation and dissociation of the cage–anion complexes, we employed ^1H NMR spectroscopy (Fig. S76–S108) to monitor the change in the composition of $CDCl_3$ solutions initially containing the "free" cages (0.3 mM) after the addition of an excess of anionic guests (3–9 mM). The observed pseudo-first-order rate constants (k_{obs}) were first calculated from plots of $\ln([A]_0/[A])$ versus time, where $[A]_0$ and $[A]$ represent the concentrations of the "free" cage at the start and at the given time after anion addition, respectively. Plots of k_{obs} versus the initial anion concentrations were then constructed. The rates of association (k_f) were defined by the slopes of these plots, while the rates of dissociation (k_b) were calculated using the equation $k_b = k_f/K_a$. For $PF_6^- \subset$ **2d**, $ClO_4^- \subset$ **2d**, $IO_4^- \subset$ **2d** and $BF_4^- \subset$ **2d**, k_f values were determined to be 30.8, 18.3, 2.3, and 11.3 $M^{-1} h^{-1}$, and k_b values were determined to be 5.5×10^{-3}, 18.3×10^{-3}, 9.2×10^{-3}, and $70.6 \times 10^{-3} h^{-1}$, respectively. In the case of $PF_6^- \subset$ **2f**, $ClO_4^- \subset$ **2f**, $IO_4^- \subset$ **2f** and $BF_4^- \subset$ **2f**, k_f values were determined to be 1.06, 1.11, 0.33, and 1.28 $M^{-1} h^{-1}$, and k_b values were determined to be 0.19×10^{-3}, 1.0×10^{-3}, 0.03×10^{-3}, and $14.2 \times 10^{-3} h^{-1}$, respectively. For each anion, both k_f and k_b of **2d** are approximately one order of magnitude larger than those of **2f**, which is consistent with the fact that, compared with the Br units in **2d**, the bulkier 4-CF_3Ph substituents in **2f** impose greater steric hindrance on the anionic guests.

Diffraction grade single crystals of $ClO_4^- \subset$ **2c**·TBA^+ (Fig. 4C) and $BF_4^- \subset$ **2c**·TBA^+ (Fig. 4D) were obtained by vapor diffusion of diisopropyl ether into their corresponding chloroform solutions, which unambiguously confirmed the formation of cage–anion complexes. The solid-state structures align with the ^1H NMR spectroscopic results recorded in solution. As expected, all the Cl substituents in the framework of **2c** are positioned outside the cage cavity, endowing the cage with a "free" cavity to accommodate the anionic guests. In the case of $ClO_4^- \subset$ **2c** and $BF_4^- \subset$ **2c**, close contacts were observed between the triazine units in the cages and the oxygen atoms (3.06 Å) in ClO_4^-, as well as the fluorine atoms (3.06 Å) of BF_4^-, indicating the occurrence of anion–π interactions. The distances between the protons in the *meta* positions relative to imine bonds and the oxygen atoms in ClO_4^- and fluorine atoms in BF_4^- were measured to be in the range of 2.55–2.83 Å, implying the formation of hydrogen bonds as secondary interactions.

The unexpected trend in anion binding affinity prompted a comprehensive computational investigation to elucidate the

physical nature of host–guest interactions. DFT calculations were initially employed to optimize the geometries of both the empty cages and their complexes with ClO_4^-. Subsequently, energy decomposition analysis (EDA) using the sobEDAw[71] method was applied to partition the total interaction energy into electrostatic, exchange-repulsion, orbital, and dispersion terms (Fig. 5A and Table S2). The analysis reveals that electrostatic components are the predominant contributions, which govern the observed total interaction energy trend of $|\Delta E_{int}(\mathbf{2b})| < |\Delta E_{int}(\mathbf{2c})| < |\Delta E_{int}(\mathbf{2d})|$ and $|\Delta E_{int}(\mathbf{2e})| < |\Delta E_{int}(\mathbf{2f})|$ (Table S2). These computational trends align closely with the experimental binding affinity. Notably, although the molecular cages are charge-neutral, the dominant electrostatic attraction likely arises from their pronounced electron-deficient character. This finding motivated us to probe deeper into the origin of the observed affinity trend.

The independent gradient model based on Hirshfeld partition of molecular density (IGMH)[72] analysis using Multiwfn 3.8(dev)[73] was employed to visualize the interfragmental interactions within the complexes. The resulting isosurfaces (Fig. 5B and S112) display broad, mainly green regions between ClO_4^- and the triazine rings, indicative of attractive anion–π interactions with a substantial dispersion character. Additionally, stronger CH–O hydrogen bond interactions are also evident as the predominately blue isosurface regions between ClO_4^- and the inward-pointing protons at the *meta*-position of the substituent groups. To quantify the contributions of these interactions, we performed quantitative assessments based on calculated quadrupole moment (for anion–π interactions) and AIM topology analysis[74] (for hydrogen bonds) (see SI, Section 6). The average quadrupole moments (Table S3) of the triazine rings for the empty cages do not correlate with the experimental affinity trend. In contrast, the cumulative hydrogen-bond energies derived from AIM analysis (Table S4) show better agreement, yet they account for only about 30% of the total interaction energy. These findings suggest that neither anion–π interactions nor hydrogen bonding serves as the primary determinant of the observed binding trend.

In an attempt to further probe the electrostatic character of the cage cavity, we analyzed the electrostatic potential (ESP) distribution[75] of the empty cages. The ESP map (Fig. 5C–E and S109), visualized on a cross-section 3 Å above the triazine plane, reveals a pronounced electropositive region within the cage cavity. Intriguingly, the intensity of this electropositive potential exhibits a clear inverse correlation with the electronegativity of the substituent groups, with the most electronegative F substituent cage **2b** having the weakest electropositive cavity. In order to clarify this counterintuitive observation, we derived restrained electrostatic potential (RESP) charges[76] for each atom. The analysis (Table S6) reveals a slight increase in the net positive charge on the triazine fragments from **2d** to **2b**, consistent with the expected inductive effect applied by the electronegative halogen substituents. Concomitantly, the twelve halogen atoms exhibit substantial negative charges, with average values increasing in the order: **2d** (−0.054 a.u.) < **2c** (−0.083 a.u.) < **2b** (−0.22 a.u.), as observed (Fig. 5F) on the ESP
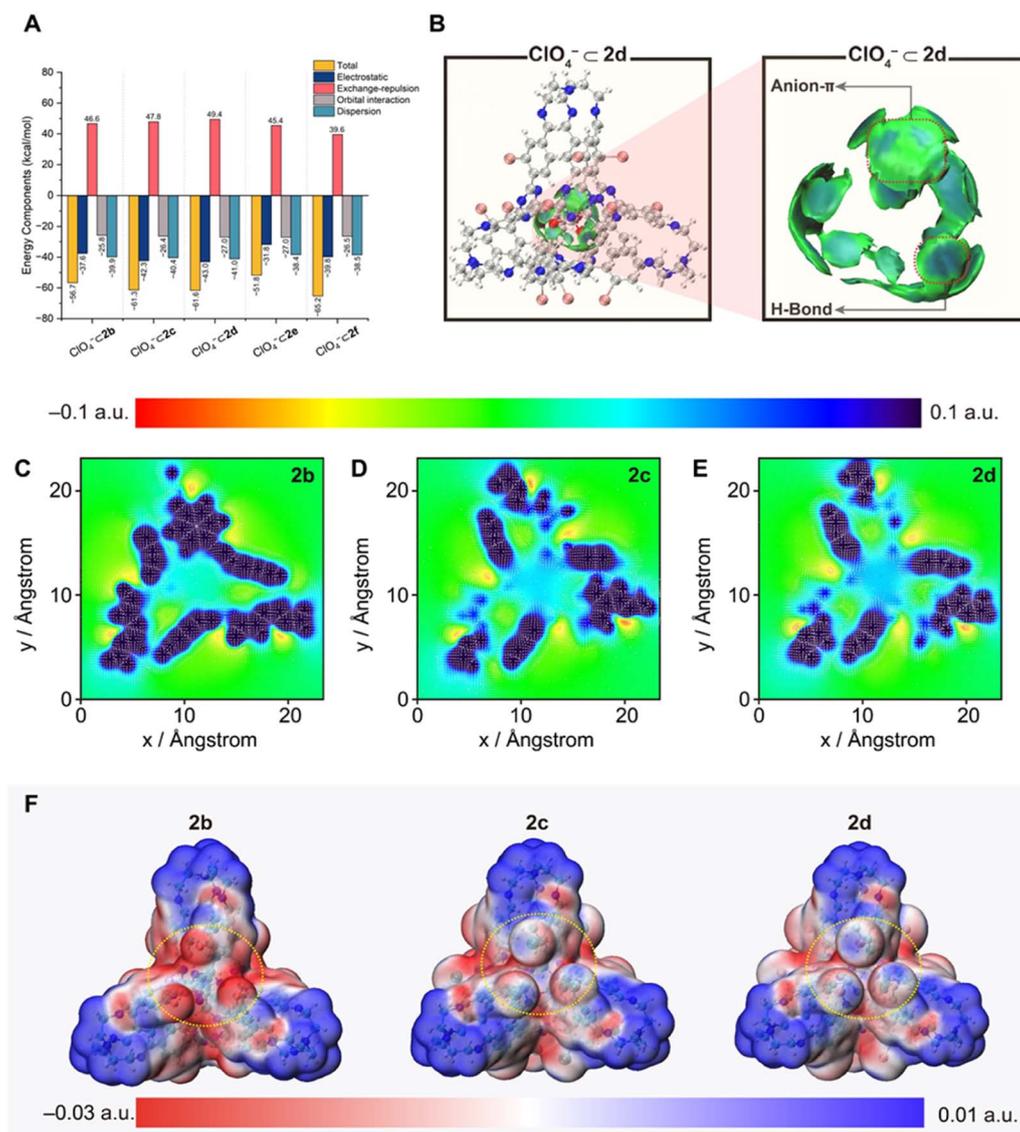
Fig. 5 (A) Energy decomposition analysis of $ClO_4^- \subset 2b$, $ClO_4^- \subset 2c$, $ClO_4^- \subset 2d$, $ClO_4^- \subset 2e$, and $ClO_4^- \subset 2f$. (B) IGMH map showing intermolecular interactions of $ClO_4^- \subset 2d$. (C–E) The 2D electrostatic potential distribution and the electric field gradient diagram of **2b** (C), **2c** (D), and **2d** (E). (F) Electrostatic potential distribution color vdW surface maps of **2b** (left), **2c** (middle), and **2d** (right).

maps, where electron-rich regions exist over the surface of the halogen atoms.

The significant negative charge localized on the fluorine atoms in **2b** motivated us to investigate their electrostatic influence by computing the electrostatic potential energy (Table S7) between cage components and an imaginary unit (-1) charge placed at the center of the cage. While the triazine units generated a notable attractive potential, it is effectively overshadowed by the repulsive potentials arising from the halogen atoms. Consequently, the net electrostatic repulsion follows the order: **2b** > **2c** > **2d**, which aligns with the experimental anion affinity series and rationalizes the primacy of the repulsive field effect exerted by the adjacent halogen atoms in governing anion binding trends.

Finally, the affinity trends for cages **2e** and **2f** are explained by complementary mechanisms. The absence of observable anion affinity of **2e** results from the electron-donating inductive effect of the Ph groups that significantly weaken the overall electrostatic term of attraction (Fig. 5A). In contrast, the strong binding affinity of **2f**, where remote CF_3 groups induce a negligible field effect, cannot be explained solely by an electron-withdrawing inductive effect. Instead, the enhanced affinity of **2f** is also attributable to the marked reduction in Pauli repulsion (Table S2). This effect arises from the decreased overlap between the occupied orbitals of the anion and **2f**, a consequence of orbital polarization induced by the electron-withdrawing CF_3 groups.

Conclusions

To summarize, condensation of a trisamino linker with a series of trisformyl precursors yielded five tetrahedral cages in modest to high yields. Each cage features four electron-deficient faces each containing a triazine unit. Three of these cages utilize their cavities to accommodate anions of complementary sizes through fourfold anion–π interactions. The substituents—all grafted at the *meta* positions relative to the formyl groups—played crucial roles in both self-assembly and anion recognition. First, they preorganized each benzaldehyde unit into a twisted dihedral angle relative to the central triazine core in the precursors. This conformation favored intramolecular CH–π interactions, which served as the key driving force for tetrahedral cage formation. Second, the electronic nature of these substituents has significant impact on anion affinity. Generally, electron-donating groups (*e.g.*, Ph) diminished binding affinity by reducing electrostatic attraction with the anionic guests. In contrast, these attractive forces were increased in cages with electron-withdrawing substituents (*e.g.*, Br, Cl, and CF$_3$-Ph), leading to enhanced anion binding. Notably, strongly electron-withdrawing substituents (*e.g.*, F) in close proximity to the binding pocket also weaken the binding affinity through a repulsive field effect. The encapsulation of anionic guests induced conformational changes in the cage framework. This, in turn, perturbed or reinforced the intramolecular CH–π interactions at each corner to a varying extent for each anion. These perturbations produced distinct NMR responses that provided characteristic signatures for differentiating between anions.

Author contributions

H. L. and Y. L. conceived the concept. Y. L. and H. T. performed the experiments and analyzed the data. P. Z. and G. W. carried out the computational studies. H. C. provided the image models. The manuscript was written through contributions of all authors. All authors have given approval to the final version of the manuscript.

Conflicts of interest

There is no conflict of interest to report.

Data availability

CCDC 2483576 and 2483577 contain the supplementary crystallographic data for this paper.[77a,b]

Supplementary information (SI): synthetic procedures, NMR spectra, ESI-MS spectra, computational details, and X-ray structure details. See DOI: https://doi.org/10.1039/d5sc08157b.

Acknowledgements

Notes and references

1 X. Yin, J. Zhang, W. Zhao, Z. Liu and J. Wang, Combined Levo-Tetrahydropalmatine and Diphenyleneiodonium Chloride Enhances Antitumor Activity in Hepatocellular Carcinoma, *Pharmacol. Res.*, 2022, **179**, 106219.

2 J. O. Lundberg, M. Carlström and E. Weitzberg, Metabolic Effects of Dietary Nitrate in Health and Disease, *Cell Metab.*, 2018, **28**, 9–22.

3 H. Yan, Q. Chen, J. Liu, Y. Feng and K. Shih, Phosphorus Recovery through Adsorption by Layered Double Hydroxide Nano-Composites and Transfer into a Struvite-Like Fertilizer, *Water Res.*, 2018, **145**, 721–730.

4 M. Long, J. Zhu, X. Wang, S. Hu, J. Zhang, K. Cheng, T. Liu, W. Liu, J. R. Reinfelder, Y. Wu and F. Li, Hematite Enhances Microbial Autotrophic Nitrate Removal in Carbonate and Phosphate-Rich Environments by Increasing Fe(II) Activity, *Sci. Total Environ.*, 2024, **949**, 175002.

5 E. Pracucci, R. T. Graham, L. Alberio, G. Nardi, O. Cozzolino, V. Pillai, G. Pasquini, L. Saieva, D. Walsh, S. Landi, J. Zhang, A. J. Trevelyan and G.-M. Ratto, Daily Rhythm in Cortical Chloride Homeostasis Underpins Functional Changes in Visual Cortex Excitability, *Nat. Commun.*, 2023, **14**, 7108.

6 B. S. Yu, P. Chen, L. H. Nie and S. Z. Yao, Determination of Chloride in Human Body Fluids by Ion Chromatography with Piezoelectric Sensor as Detector, *Anal. Lett.*, 1996, **29**, 43–57.

7 Y. Liu, W. Zhao, C.-H. Chen and A. H. Flood, Chloride Capture Using a C–H Hydrogen-Bonding Cage, *Science*, 2019, **365**, 159–161.

8 X. Wu, P. Wang, P. Turner, W. Lewis, O. Catal, D. S. Thomas and P. A. Gale, Tetraurea Macrocycles: Aggregation-Driven Binding of Chloride in Aqueous Solutions, *Chem*, 2019, **5**, 1210–1222.

9 M. A. Yawer, V. Havel and V. Sindelar, A Bambusuril Macrocycle That Binds Anions in Water with High Affinity and Selectivity, *Angew Chem. Int. Ed. Engl.*, 2015, **54**, 276–279.

10 X. Zhao, H. Wang, B. Li, W. Zhang, X. Li, W. Zhao, C. Janiak, A. W. Heard, X.-J. Yang and B. Wu, A Hydrogen-Bonded Ravel Assembled by Anion Coordination, *Angew. Chem., Int. Ed.*, 2022, **61**, e202115042.

11 H. Wang, S. Fang, G. Wu, Y. Lei, Q. Chen, H. Wang, Y. Wu, C. Lin, X. Hong, S. K. Kim, J. L. Sessler and H. Li, Constraining Homo- and Heteroanion Dimers in Ultraclose Proximity within a Self-Assembled Hexacationic Cage, *J. Am. Chem. Soc.*, 2020, **142**, 20182–20190.

12 L. Jing, E. Deplazes, J. K. Clegg and X. Wu, A Charge-Neutral Organic Cage Selectively Binds Strongly Hydrated Sulfate Anions in Water, *Nat. Chem.*, 2024, **16**, 335–342.

13 P. A. Gale, J. L. Sessler, V. Král and V. Lynch, Calix[4]Pyrroles: Old yet New Anion-Binding Agents, *J. Am. Chem. Soc.*, 1996, **118**, 5140–5141.

14 A. P. Bisson, V. M. Lynch, M.-K. C. Monahan and E. V. Anslyn, Recognition of Anions through NH–π Hydrogen Bonds in a Bicyclic Cyclophane—Selectivity for Nitrate, *Angew Chem. Int. Ed. Engl.*, 1997, **36**, 2340–2342.

15 M. Chvojka, D. Madea, H. Valkenier and V. Šindelář, Tuning Ch Hydrogen Bond-Based Receptors toward Picomolar Anion Affinity Via the Inductive Effect of Distant Substituents, *Angew. Chem., Int. Ed.*, 2024, **63**, e202318261.

16 R. Custelcean, A. Bock and B. A. Moyer, Selectivity Principles in Anion Separation by Crystallization of Hydrogen-Bonding Capsules, *J. Am. Chem. Soc.*, 2010, **132**, 7177–7185.

17 J. Pancholi and P. D. Beer, Halogen Bonding Motifs for Anion Recognition, *Coord. Chem. Rev.*, 2020, **416**, 213281.

18 J. T. Wilmore and P. D. Beer, Exploiting the Mechanical Bond Effect for Enhanced Molecular Recognition and Sensing, *Adv. Mater.*, 2024, **36**, 2309098.

19 M. J. Langton, S. W. Robinson, I. Marques, V. Félix and P. D. Beer, Halogen Bonding in Water Results in Enhanced Anion Recognition in Acyclic and Rotaxane Hosts, *Nat. Chem.*, 2014, **6**, 1039–1043.

20 A. M. S. Riel, D. A. Decato, J. Sun, C. J. Massena, M. J. Jessop and O. B. Berryman, Correction: The Intramolecular Hydrogen Bonded–Halogen Bond: A New Strategy for Preorganization and Enhanced Binding, *Chem. Sci.*, 2018, **9**, 6451.

21 M. G. Sarwar, B. Dragisic, L. J. Salsberg, C. Gouliaras and M. S. Taylor, Thermodynamics of Halogen Bonding in Solution: Substituent, Structural, and Solvent Effects, *J. Am. Chem. Soc.*, 2010, **132**, 1646–1653.

22 M. G. Sarwar, B. Dragisic, S. Sagoo and M. S. Taylor, A Tridentate Halogen-Bonding Receptor for Tight Binding of Halide Anions, *Angew. Chem., Int. Ed.*, 2010, **49**, 1674–1677.

23 N. L. Kilah, M. D. Wise, C. J. Serpell, A. L. Thompson, N. G. White, K. E. Christensen and P. D. Beer, Enhancement of Anion Recognition Exhibited by a Halogen-Bonding Rotaxane Host System, *J. Am. Chem. Soc.*, 2010, **132**, 11893–11895.

24 F. Zapata, A. Caballero, N. G. White, T. D. W. Claridge, P. J. Costa, V. t. Félix and P. D. Beer, Fluorescent Charge-Assisted Halogen-Bonding Macrocyclic Halo-Imidazolium Receptors for Anion Recognition and Sensing in Aqueous Media, *J. Am. Chem. Soc.*, 2012, **134**, 11533–11541.

25 A. Caballero, F. Zapata, N. G. White, P. J. Costa, V. Félix and P. D. Beer, A Halogen-Bonding Catenane for Anion Recognition and Sensing, *Angew. Chem., Int. Ed.*, 2012, **51**, 1876–1880.

26 M. Cametti, K. Raatikainen, P. Metrangolo, T. Pilati, G. Terraneo and G. Resnati, 2-Iodo-Imidazolium Receptor Binds Oxoanionsvia Charge-Assisted Halogen Bonding, *Org. Biomol. Chem.*, 2012, **10**, 1329–1333.

27 C. Xu, Q. G. Tran, D. Liu, C. Zhai, L. Wojtas and W. Liu, Charge-Assisted Hydrogen Bonding in a Bicyclic Amide Cage: An Effective Approach to Anion Recognition and Catalysis in Water, *Chem. Sci.*, 2024, **15**, 16040–16049.

28 Y. Wu, C. Zhang, S. Fang, D. Zhu, Y. Chen, C. Ge, H. Tang and H. Li, A Self-Assembled Cage Binding Iodide Anions over Other Halide Ions in Water, *Angew. Chem., Int. Ed.*, 2022, **61**, e202209078.

29 E. G. Percástegui, J. Mosquera and J. R. Nitschke, Anion Exchange Renders Hydrophobic Capsules and Cargoes Water-Soluble, *Angew. Chem., Int. Ed.*, 2017, **56**, 9136–9140.

30 W. Liu, L. O. Jones, H. Wu, C. L. Stern, R. A. Sponenburg, G. C. Schatz and J. F. Stoddart, Supramolecular Gold Stripping from Activated Carbon Using A-Cyclodextrin, *J. Am. Chem. Soc.*, 2021, **143**, 1984–1992.

31 T. Fiala, K. Sleziakova, K. Marsalek, K. Salvadori and V. Sindelar, Thermodynamics of Halide Binding to a Neutral Bambusuril in Water and Organic Solvents, *J. Org. Chem.*, 2018, **83**, 1903–1912.

32 M. Lisbjerg, B. E. Nielsen, B. O. Milhøj, S. P. A. Sauer and M. Pittelkow, Anion Binding by Biotin[6]Uril in Water, *Org. Biomol. Chem.*, 2015, **13**, 369–373.

33 Q.-Y. Hong, B. Huang, M.-X. Wu, J.-Y. Jiang, H.-B. Yang, X.-L. Zhao, G. H. Clever and X. Shi, Self-Assembly, Interlocking, Interconversion and Anion-Binding Catalysis in Phenoxazine-Based Pd$_2$L$_4$ and Pd$_4$L$_8$ Coordination Cages, *Nat. Commun.*, 2025, **16**, 2484.

34 S. Löffler, J. Lübben, L. Krause, D. Stalke, B. Dittrich and G. H. Clever, Triggered Exchange of Anionic for Neutral Guests inside a Cationic Coordination Cage, *J. Am. Chem. Soc.*, 2015, **137**, 1060–1063.

35 S. Sudan, D. W. Chen, C. Berton, F. Fadaei-Tirani and K. Severin, Synthetic Receptors with Micromolar Affinity for Chloride in Water, *Angew. Chem., Int. Ed.*, 2023, **62**, e202218072.

36 W.-L. Jiang, B. Huang, X.-L. Zhao, X. Shi and H.-B. Yang, Strong Halide Anion Binding within the Cavity of a Conformation-Adaptive Phenazine-Based Pd$_2$L$_4$ Cage, *Chem*, 2023, **9**, 2655–2668.

37 S. M. Butler, D. M. Beagan, W. Lewis, N. K. Szymczak and K. A. Jolliffe, Gem-Diboronic Acids: A Motif for Anion Recognition in Competitive Media, *Angew. Chem., Int. Ed.*, 2025, **64**, e202502582.

38 A. Frontera, P. Gamez, M. Mascal, T. J. Mooibroek and J. Reedijk, Putting Anion–π Interactions into Perspective, *Angew. Chem., Int. Ed.*, 2011, **50**, 9564–9583.

39 P. Gamez, The Anion–π Interaction: Naissance and Establishment of a Peculiar Supramolecular Bond, *Inorg. Chem. Front.*, 2014, **1**, 35–43.

40 Y. Cotelle, V. Lebrun, N. Sakai, T. R. Ward and S. Matile, Anion-π Enzymes, *ACS Cent. Sci.*, 2016, **2**, 388–393.

41 D.-X. Wang and M.-X. Wang, Exploring Anion−π Interactions and Their Applications in Supramolecular Chemistry, *Acc. Chem. Res.*, 2020, **53**, 1364–1380.

42 D. Quiñonero, C. Garau, C. Rotger, A. Frontera, P. Ballester, A. Costa and P. M. Deyà, *Angew. Chem., Int. Ed.*, 2002, **114**, 3539–3542.

43 M. Mascal, A. Armstrong and M. D. Bartberger, Anion−Aromatic Bonding: A Case for Anion Recognition by π-Acidic Rings, *J. Am. Chem. Soc.*, 2002, **124**, 6274–6276.

44 I. Alkorta, I. Rozas and J. Elguero, Interaction of Anions with Perfluoro Aromatic Compounds, *J. Am. Chem. Soc.*, 2002, **124**, 8593–8598.

45 P. Ballester, Experimental Quantification of Anion−π Interactions in Solution Using Neutral Host–Guest Model Systems, *Acc. Chem. Res.*, 2013, **46**, 874–884.

46 D.-X. Wang and M.-X. Wang, Anion−π Interactions: Generality, Binding Strength, and Structure, *J. Am. Chem. Soc.*, 2013, **135**, 892–897.

47 N. Bar Ziv, C. Chen, B. da Camara, R. R. Julian and R. J. Hooley, Selective Aqueous Anion Recognition in an Anionic Host, *iScience*, 2024, **27**, 111348.

48 A. Ferguson, R. W. Staniland, C. M. Fitchett, M. A. Squire, B. E. Williamson and P. E. Kruger, Variation of Guest Selectivity within [Fe₄L₄]⁸⁺ Tetrahedral Cages through Subtle Modification of the Face-Capping Ligand, *Dalton Trans.*, 2014, **43**, 14550–14553.

49 B. da Camara, N. B. Ziv, V. Carta, G. A. Mota Orozco, H.-T. Wu, R. R. Julian and R. J. Hooley, Gated, Selective Anion Exchange in Functionalized Self-Assembled Cage Complexes, *Chem.–Eur. J.*, 2023, **29**, e202203588.

50 A. B. Grommet and J. R. Nitschke, Directed Phase Transfer of an FeII₄L₄ Cage and Encapsulated Cargo, *J. Am. Chem. Soc.*, 2017, **139**, 2176–2179.

51 L. Xu, D. Zhang, T. K. Ronson and J. R. Nitschke, Improved Acid Resistance of a Metal–Organic Cage Enables Cargo Release and Exchange between Hosts, *Angew. Chem., Int. Ed.*, 2020, **59**, 7435–7438.

52 A. M. Castilla, T. K. Ronson and J. R. Nitschke, Sequence-Dependent Guest Release Triggered by Orthogonal Chemical Signals, *J. Am. Chem. Soc.*, 2016, **138**, 2342–2351.

53 D. X. Wang, Q. Y. Zheng, Q. Q. Wang and M. X. Wang, Halide Recognition by Tetraoxacalix[2]Arene[2]Triazine Receptors: Concurrent Noncovalent Halide−π and Lone-Pair−π Interactions in Host–Halide–Water Ternary Complexes, *Angew. Chem., Int. Ed.*, 2008, **47**, 7485–7488.

54 S.-Y. Zhuang, Y. Cheng, Q. Zhang, S. Tong and M.-X. Wang, Synthesis of I-Corona[6]Arenes for Selective Anion Binding: Interdependent and Synergistic Anion−π and Hydrogen-Bond Interactions, *Angew. Chem., Int. Ed.*, 2020, **59**, 23716–23723.

55 X.-D. Wang, Q.-Q. Wang, Y.-F. Ao and D.-X. Wang, Conformational Control of Oxacalix[3]Arene[3]Triazine with Anion−π Interactions, *Cryst. Growth Des.*, 2018, **18**, 2707–2711.

56 J. Luo, J. Zhu, D.-H. Tuo, Q. Yuan, L. Wang, X.-B. Wang, Y.-F. Ao, Q.-Q. Wang and D.-X. Wang, Macrocycle-Directed Construction of Tetrahedral Anion−π Receptors for Nesting Anions with Complementary Geometry, *Chem.–Eur. J.*, 2019, **25**, 13275–13279.

57 D.-X. Wang, Q.-Y. Zheng, Q.-Q. Wang and M.-X. Wang, Halide Recognition by Tetraoxacalix[2]Arene[2]Triazine Receptors: Concurrent Noncovalent Halide−π and Lone-Pair−π Interactions in Host–Halide–Water Ternary Complexes, *Angew. Chem., Int. Ed.*, 2008, **47**, 7485–7488.

58 Y. Chen, H. Tang, H. Chen and H. Li, Self-Assembly Via Condensation of Imine or Its N-Substituted Derivatives, *Acc. Chem. Res.*, 2023, **56**, 2838–2850.

59 T. Jiao, L. Chen, D. Yang, X. Li, G. Wu, P. Zeng, A. Zhou, Q. Yin, Y. Pan, B. Wu, X. Hong, X. Kong, V. M. Lynch, J. L. Sessler and H. Li, Trapping White Phosphorus within a Purely Organic Molecular Container Produced by Imine Condensation, *Angew. Chem., Int. Ed.*, 2017, **56**, 14545–14550.

60 T. Jiao, H. Qu, L. Tong, X. Cao and H. Li, A Self-Assembled Homochiral Radical Cage with Paramagnetic Behaviors, *Angew. Chem., Int. Ed.*, 2021, **60**, 9852–9858.

61 Y. Chen, G. Wu, B. Chen, H. Qu, T. Jiao, Y. Li, C. Ge, C. Zhang, L. Liang, X. Zeng, X. Cao, Q. Wang and H. Li, Self-Assembly of a Purely Covalent Cage with Homochirality by Imine Formation in Water, *Angew. Chem., Int. Ed.*, 2021, **60**, 18815–18820.

62 Y. Chen, Z. Cao, T. Feng, X. Zhang, Z. Li, X. Dong, S. Huang, Y. Liu, X. Cao, A. C. H. Sue, C. Peng, X. Lin, L. Wang and H. Li, Enantioselective Self-Assembly of a Homochiral Tetrahedral Cage Comprising Only Achiral Precursors, *Angew. Chem., Int. Ed.*, 2024, **63**, e202400467.

63 H. Tang, Y. Lu, Y. Qian, C. Ge, J. Liu, H. Chen and H. Li, A Conformationally Adaptable Tetrahedral Cage with Different Guest Encapsulation Models, *Chem. Sci.*, 2025, **16**, 10867–10873.

64 T. Jiao, G. Wu, L. Chen, C.-Y. Wang and H. Li, Precursor Control over the Self-Assembly of Organic Cages Via Imine Condensation, *J. Org. Chem.*, 2018, **83**, 12404–12410.

65 S. Lee, C.-H. Chen and A. H. Flood, A Pentagonal Cyanostar Macrocycle with Cyanostilbene CH Donors Binds Anions and Forms Dialkylphosphate [3]Rotaxanes, *Nat. Chem.*, 2013, **5**, 704–710.

66 M. K. Deliomeroglu, V. M. Lynch and J. L. Sessler, Conformationally Switchable Non-Cyclic Tetrapyrrole Receptors: Synthesis of Tetrakis(1H-Pyrrole-2-Carbaldehyde) Derivatives and Their Anion Binding Properties, *Chem. Commun.*, 2014, **50**, 11863–11866.

67 M. K. Deliomeroglu, V. M. Lynch and J. L. Sessler, Non-Cyclic Formylated Dipyrromethanes as Phosphate Anion Receptors, *Chem. Sci.*, 2016, **7**, 3843–3850.

68 D. X. Wang, Q. Q. Wang, Y. Han, Y. Wang, Z. T. Huang and M. X. Wang, Versatile Anion−π Interactions between Halides and a Conformationally Rigid Bis(Tetraoxacalix[2]Arene[2] Triazine) Cage and Their Directing Effect on Molecular Assembly, *Chem.–Eur. J.*, 2010, **16**, 13053–13057.

69 X.-Y. Wang, J. Zhu, Q.-Q. Wang, Y.-F. Ao and D.-X. Wang, Anion−π-Directed Self-Assembly between Di- and Trisulfonates and a Rigid Molecular Cage with Three Electron-Deficient V-Clefts, *Inorg. Chem.*, 2019, **58**, 5980–5987.

70 V. Havel, M. A. Yawer and V. Sindelar, Real-Time Analysis of Multiple Anion Mixtures in Aqueous Media Using a Single Receptor, *Chem. Commun.*, 2015, **51**, 4666–4669.

71 T. Lu and Q. Chen, Simple, Efficient, and Universal Energy Decomposition Analysis Method Based on Dispersion-Corrected Density Functional Theory, *J. Phys. Chem. A*, 2023, **127**, 7023–7035.

72 T. Lu and Q. Chen, Independent Gradient Model Based on Hirshfeld Partition: A New Method for Visual Study of

Interactions in Chemical Systems, *J. Comput. Chem.*, 2022, **43**, 539–555.

73 T. Lu and F. Chen, Multiwfn: A Multifunctional Wavefunction Analyzer, *J. Comput. Chem.*, 2012, **33**, 580–592.

74 E. Espinosa, E. Molins and C. Lecomte, Hydrogen Bond Strengths Revealed by Topological Analyses of Experimentally Observed Electron Densities, *Chem. Phys. Lett.*, 1998, **285**, 170–173.

75 J. Zhang and T. Lu, Efficient Evaluation of Electrostatic Potential with Computerized Optimized Code, *Phys. Chem. Chem. Phys.*, 2021, **23**, 20323–20328.

76 C. I. Bayly, P. Cieplak, W. Cornell and P. A. Kollman, A Well-Behaved Electrostatic Potential Based Method Using Charge Restraints for Deriving Atomic Charges: The Resp Model, *J. Phys. Chem.*, 1993, **97**, 10269–10280.

77 (*a*) CCDC 2483576: Experimental Crystal Structure Determination, 2026, DOI: 10.5517/ccdc.csd.cc2pccct.; (*b*) CCDC 2483577: Experimental Crystal Structure Determination, 2026, DOI: 10.5517/ccdc.csd.cc2pccdv.